Optimization-based queue estimation on an arterial traffic link with measurement uncertainties

Leah A. Anderson (corresponding author)
University of California, Berkeley
Partners for Advanced Transportation Technology, Connected Corridors Program
2105 Bancroft Way, Third Floor; Berkeley, CA 94720-3830
phone: (510) 642-4522, fax: (510) 642-0910, email: leah.anderson@berkeley.edu

Edward S. Canepa
King Abdullah University of Science and Technology
4700 KAUST, Thuwal; Jeddah, Saudi Arabia
email: edward.canepa@kaust.edu.sa

Roberto Horowitz
University of California, Berkeley
5138 Etcheverry Hall, Mailstop 1740; Berkeley, CA 94720-1740
phone: (510) 642-4675, fax: (510) 642-0910, email: horowitz@me.berkeley.edu

Christian G. Claudel
King Abdullah University of Science and Technology
4700 KAUST, Thuwal; Jeddah, Saudi Arabia
email: christian.claudel@kaust.edu.sa

Alexandre M. Bayen
University of California, Berkeley
642 Sutardja Hall (CITRIS); Berkeley, CA 94720-1710
phone: (510) 642-2468, fax: (510) 643-5264, email: bayen@berkeley.edu

Paper submitted to TRB Annual Meeting 2014
August 1, 2013

4748 words + 8 figure(s) + 1 table(s) ⇒ 6998 'words'

ABSTRACT

Advanced monitoring and control of arterial road traffic network operations requires accurate knowledge of current and predicted performance measures on the network. Recently studied signal control algorithms, for example, use the lengths of vehicle queues for each turning movement to determine how subsequent signal cycles should be distributed into phases. This article presents a queue estimation procedure which can integrate measurements from classical count or occupancy sensors into a single physical model of general link state and queue length in particular. We show how realistic data from an arterial link can be used to estimate the current or recent state of this link by manipulating the initial and boundary conditions used in an explicit solution to the Moskowitz (cumulative number of vehicles) formulation of the Lighthill-Whitham-Richards (LWR) partial differential equation. We demonstrate the results of this estimation procedure using various sensor configurations extracted from data and ground-truth vehicle trajectories taken from the NGSIM community's Lankershim Blvd data set.

INTRODUCTION

Numerous advanced traffic responsive arterial signalization management schemes rely on the accurate estimation of vehicle queue lengths and turning ratios (*1, 2, 3*). Queue length estimation is also necessary in traffic responsive on-ramp metering schemes (*4*). However, direct measurement of queue lengths is difficult in practice. While the desired measurements can potentially be obtained using video feeds, this is not always feasible due to visibility constraints, image processing accuracy, and maintenance costs. Several proposed onramp queue estimation algorithms rely on vehicle detectors physically installed in the roadway. An analysis, experimental verification and comparison of several on-ramp queue estimation algorithms is presented in (*5*).

Several queue estimation schemes rely on counting vehicles entering and leaving the queue. This method is known to introduce significant errors into the queue estimates due to its inability to correct for offsets introduced by vehicle miscounts an incorrect estimates of the queue's initial length (*6, 7, 8*). Work has been done to improve the performance of this queue estimation approach by incorporating occupancy measurements (*8, 9, 7*), or by introducing heuristic volume adjustment mechanisms (*6, 7*) or statistical analyses (*10*). In (*5*) the vehicle re-identification techniques using magnetometer sensor arrays (*11*) are used to match vehicles entering and exiting the queues in order to correct for offsets in counting vehicles entering and leaving the queue. The re-identification algorithm is subsequently modified in (*12*) in order to improve the re-identification accuracy of slowly-moving vehicles, and was experimentally shown to provide adequate on-ramp queues estimates (*13*). Vehicle re-identification techniques have also been used to estimate queues on arterials (*13*). Unfortunately, most successful re-identification techniques rely on the use of specialized magnetometer arrays that are not yet widely available in many arterial streets.

Statistical approaches to estimation are often used to try to overcome the lack of physical measurements and high variability on urban roads (*14, 15*) Some even using GPS-probe data to derive statistical queue estimates from individual vehicle trajectories (*16, 17, 18, 19*). These algorithms are also limited by sparsely available data, unrealistic assumptions about vehicle arrival patterns, and a lack of precision.

Here we present a new method for queue length estimation on arterial links based on a macroscopic horizontal queuing model (*20*). Because it only depends on aggregate measurements and a macroscopic flow model to determine a "best fit" of link state given a known bound on measurement error, it is less sensitive to imprecise or erroneous measurements than some other queue estimation techniques. While our method can utilize measurements from traditional in-road sensors, it can also integrate measurements from advanced sensing systems such as re-identification or travel time monitors when they are available. In related work, the same techniques have been used with trajectory or position data; for example from GPS-enabled smartphones (*21*).

We model an arterial link using the *Lighthill-Whitham-Richards* (LWR) partial differential equation (*22, 23*). Others have demonstrated the ability of this kinematic model to predict and control arterial traffic (*24, 25*). Here we use this theory to seek an explicit expression for a function describing the density state of an arterial link. This solution is obtained using a Hamilton-Jacobi formulation of the LWR equation known as the Moskowitz formulation (*26*). The Moskowitz model is well-studied within the freeway traffic flow community, and thus there are many known solution methodologies. In the present work, we chose to use a class of weak solutions known as the *Barron-Jensen/Frankowska* (B-J/F) solutions (*27*). Because we are able to find an explicit analytical solution for traffic state, we can operate on any spatial or temporal resolution of sensor data without the need for mapping measurements to a discretized grid.

Measurements are incorporated into our solutions via choice of initial and/or boundary conditions. As previously presented in the context of freeways in (*21*), we choose boundary flows that optimize some desired convex function of the unknown value conditions within constraints imposed both by the kinematic dynamics of the LWR PDE and the available measurements. The objective of this algorithm is therefore to generate a realistic estimation of the aggregate traffic flow behaviors over the measured time horizon which could feasibly generate the included observations–fulfilling both an estimation and data reconciliation functionality. Yet our work varies from classical approaches to estimation such as the Kalman filter: instead of iteratively finding the state estimate that minimizes least square measurement error, we seek a one-shot solution which does satisfy all available measurements but primarily optimizes an objective function designed to represent the most likely link dynamics that are "unknown" or left unconstrained by existing measurements.

We would like to emphasize that our objective is to reconstruct a general "averaged" measure of queuing behaviors and demands for the purposes of immediate estimation and control actuation. While others have studied means of adjusting macroscopic modeling to account for behavioral and higher-order dynamic effects (*28*), we do not attempt to reconstruct microscopic or even lane-specific behaviors.

We analyze the results of our LWR estimator given various combinations of magnetic loop detectors and point-to-point travel time measurements. Specifically, we compare the estimated queue lengths generated by model outputs to ground-truth measurements from a set of vehicle trajectory data captured from video recordings along a section of Lankershim Boulevard in Los Angeles, California. This open-source data was made available by the Next Generation Simulation Community (NGSIM), a project of the Federal Highway Administration.

The problem we are addressing is further detailed in Section 3, followed by a description of the model and procedures used for the estimation algorithm in Section 4. Section 5 describes the raw data and processing methods we used to simulate two types of sensor data: counts of entering vehicles, and end-to-end link travel time measurements. Numerical results are then analyzed in Section 6. We conclude with a comparison of model results using the two previously mentioned sources of data.

PROBLEM FORMULATION

We consider an arterial road link defined between spatial locations ξ and χ. This link is unidirectional, has a constant number of lanes l along its entire domain, and traffic can only enter or exit at the upstream and downstream link boundaries (respectively).

We define the state of this link $\rho(t,x)$ to be the evolution of spatial density of the link for all locations $x \in [\xi, \chi]$ at all times $t \in [t_{\min}, t_{\max}]$. For known link parameters freeflow velocity v, shockwave (or queue dissipation) speed w, and critical density ρ_c, the flow $f(t,x)$ of vehicles across a single point x is described by a function $\psi(\rho(t,x))$ of link state, as follows:

$$f(t,x) = \psi(\rho(t,x)) \tag{1}$$

$$= \begin{cases} v\rho & \text{if } \rho \leq \rho_c \\ w(\rho - \rho_c) & \text{otherwise} \end{cases} \tag{2}$$

This piecewise-linear relationship between flow and density is commonly known as the *flux function*, or triangular *fundamental diagram*, derived through empirical observation of traffic dynamics.

It is employed in many widely accepted macroscopic traffic flow models.

The road segment is bounded downstream (at $x = \chi$) by a traffic signal which can influence link state by impeding link outflow for fixed time durations. The time t_{red} at which downstream flow is artificially restricted is known ($f(\chi, t_{\text{red}}) = 0$).

ESTIMATION ALGORITHM

Incorporating multiple measurements into a single estimation of traffic state requires a fundamental physical model of traffic dynamics. The evolution of traffic state $\rho(t, x)$ is commonly described using the LWR model. This is a first-order *partial differential equation* (PDE) which is derived by applying the principle of mass conservation to the flow of traffic across a finite region using an empirical flux function such as the one described in equation (1):

$$\frac{\partial \rho(t,x)}{\partial t} + \frac{\partial \psi(\rho(t,x))}{\partial x} = 0 \tag{3}$$

While the LWR model in this form presents a commonly used description of aggregate traffic dynamics, it is difficult to assimilate measurements of internal flows or individual trajectories into such a model due to its representation of density as a continuous aggregated quantity. In addition, the non-smoothness of its solution creates challenges for estimation (*29, 30*). We therefore represent traffic state using a modification of this PDE known as the *Moskowitz* or *cumulative number of vehicles* equation (*31, 32*).

Consider a function $\mathbf{M}(t, x)$ defined such that its spatial derivative is equal to the negative of the equation defining spatial density on a road link, and its temporal derivative is equivalent to the equation describing the resulting traffic flow:

$$\frac{\partial \mathbf{M}(t,x)}{\partial x} = -\rho(t,x) \tag{4}$$

$$\frac{\partial \mathbf{M}(t,x)}{\partial t} = f(t,x) = \psi(\rho(t,x)) \tag{5}$$

The Moskowitz function $\mathbf{M}(t, x)$ can be physically interpreted as describing the flow of vehicles through space $x \in [\xi, \chi]$ by assigning consecutive integer labels to vehicles entering a link at $x = \xi$ and tracing the trajectory of those vehicles over time. If the vehicle labeled n is at location x' at time t', $\lfloor \mathbf{M}(t', x') \rfloor = n$. Via integration of $\rho(t, x)$, equation (3) can be rewritten in terms of $\mathbf{M}(t, x)$ as follows:

$$\frac{\partial \mathbf{M}(t,x)}{\partial t} + \psi\left(-\frac{\partial \mathbf{M}(t,x)}{\partial x}\right) = 0 \tag{6}$$

This transformation of the LWR PDE is in the form of a *Hamilton-Jacobi* PDE (HJ-PDE) with the flux function $\psi(\rho)$ serving as the Hamiltonian. There are several known methodologies for finding weak solutions to Hamilton-Jacobi PDEs, one of which we will utilize in this work.

Mathematical Framework

To find the solution to any PDE, one must have defined a set of initial and/or boundary conditions for the solution to satisfy. Here we define the concept of a *value condition* to encompass the common notions of initial, boundary, and internal conditions. A value condition $\mathbf{c}(\cdot, \cdot)$ is defined as

a lower semicontinuous function defined on some subset of domain $[0, t_{\max}] \times [\xi, \chi]$. Any solution to the PDE being investigated must satisfy all associated value conditions on their respective domains.

In this work, the value conditions $\mathbf{c}_j$ are not known specifically but rather must be estimated before solving the LWR PDE. Chosen conditions must not only satisfy the physical limitations imposed by the model, but also permit the feasibility of any available measurements of network state. We therefore use the following framework to develop constraints on the set of feasible value conditions.

This work specifically employs a class of weak solutions to HJ-PDEs known as the *Barron-Jensen/Frankowska* (B-J/F) solutions. These solutions are represented by the *Lax-Hopf formula* (*32*, *33*): for value condition $\mathbf{c}_j(\cdot, \cdot)$,

$$\mathbf{M}_{\mathbf{c}}(t, x) = \inf_{(u,T) \in \text{Dom}\,(\varphi^*) \times \mathbb{R}^+} \left(\mathbf{c}(t - T, x + Tu) + T\varphi^*(u)\right) \tag{7}$$

where $\varphi^*(\cdot)$ is the *Legendre-Fenchel transform* of Hamiltonian $\psi(\cdot)$, defined by

$$\varphi^*(u) := \sup_{p \in \text{Dom}(\psi)} \left[p \cdot u + \psi(p)\right] \tag{8}$$

Note that while equation (7) implies that $\mathbf{M}_{\mathbf{c}}(\cdot, \cdot)$ exists for any $\mathbf{c}$, this solution is not guaranteed to be compatible with the corresponding value condition. In other words, it is not necessarily true that $\forall (t, x) \in \text{Dom}(\mathbf{c}),\ \mathbf{M}_{\mathbf{c}}(t, x) = \mathbf{c}(t, x)$. To account for this, note that the structure of equation (7) implies the *inf-morphism* property: let $\mathbf{c}(\cdot, \cdot)$ be a minimum of a finite number of lower semicontinuous functions,

$$\forall (t, x) \in [0, t_{\max}] \times [\xi, \chi]\,,\ \mathbf{c}(t, x) := \min_{j \in J} \mathbf{c}_j(t, x) \tag{9}$$

Then $\mathbf{M}_{\mathbf{c}}$ can be decomposed as

$$\forall (t, x) \in [0, t_{\max}] \times [\xi, \chi]\,,\ \mathbf{M}_{\mathbf{c}}(t, x) = \min_{j \in J} \mathbf{M}_{\mathbf{c}_j}(t, x) \tag{10}$$

For reference on the inf-morphism property, see (*33*).

To then ensure that all value conditions used to find the LWR solution will apply in the strong sense, we must use the inf-morphism property to define "model constraints" on these conditions $\mathbf{c}_j(\cdot, \cdot)$: the value condition $\mathbf{c}(\cdot, \cdot) = \min_{j \in J} \mathbf{c}_j(\cdot, \cdot)$, satisfies $\forall (t, x) \in \text{Dom}(\mathbf{c})$, $\mathbf{M}_{\mathbf{c}}(t, x) = \mathbf{c}(t, x)$ if and only if

$$\mathbf{M}_{\mathbf{c}_j}(t, x) \geq \mathbf{c}_i(t, x)\ \forall (t, x) \in \text{Dom}(\mathbf{c}_i),\ \forall (i, j) \in J^2 \tag{11}$$

The model constraints are further defined in section 4.3.

Furthermore, we must ensure that the value conditions used to solve the LWR model can satisfy all known measurements within their stated error bounds. This requires the introduction of a set of "data constraints" which encode the information collected from network sensors into convex inequality constraints. Examples of data constraints are introduced in section 4.4.

Initial and Boundary Conditions

Assume the following affine initial and upstream/downstream boundary conditions, defined for discrete spatial blocks k of length X and discrete time blocks n of length T:

initial condition:

$$M_k(t,x) = \begin{cases} -\sum_{i=0}^{k-1} \rho(i)X - \rho(k)(x-kX) & \text{if } t=0 \text{ and } x \in [kX,(k+1)X] \\ +\infty & \text{otherwise} \end{cases} \tag{12}$$

upstream condition:

$$\gamma_n(t,x) = \begin{cases} \sum_{i=0}^{n-1} f_{\text{in}}(i)T + f_{\text{in}}(n)(t-nT) & \text{if } x=\xi \text{ and } t \in [nT,(n+1)T] \\ +\infty & \text{otherwise} \end{cases} \tag{13}$$

downstream condition:

$$\beta(t,x) = \begin{cases} \sum_{i=0}^{n-1} f_{\text{out}}(i)T + f_{\text{out}}(n)(t-nT) & \\ \qquad\qquad - \sum_{k=0}^{k_{\max}} \rho(k)(x-kX) & \text{if } x=\chi \text{ and } t \in [nT,(n+1)T] \\ +\infty & \text{otherwise} \end{cases} \tag{14}$$

A direct application of equation (7) on (12)-(14) yields the following solutions (following the approach of (*33*)):

$$\mathbf{M}_{M_k} = \begin{cases} +\infty & \text{if } x \le kX+wt \text{ or } x \ge (k+1)X+vt \\ -\sum_{i=0}^{k-1} \rho(i)X + \rho_c(tv+kX-x) & \text{if } kX+tw \le x \le kX+tv \\ -\sum_{i=0}^{k-1} \rho(i)X + \rho(k)(tv+kX-x) & \text{if } kX+tv \le x \le (k+1)X+tv \\ -\sum_{i=0}^{k} \rho(i)X + \rho_c(tw+(k+1)X-x) - \rho_m tw & \text{if } (k+1)X+tw \le x \le (k+1)X+tw \\ -\sum_{i=0}^{k-1} \rho(i)X + \rho(k)(tw+kX-x) - \rho_m tw & \text{if } kX+tw \le x \le (k+1)X+tv \end{cases} \tag{15}$$

$$\mathbf{M}_{\gamma_n} = \begin{cases} +\infty & \text{if } t \le nT + \frac{x-\xi}{v} \\ \sum_{i=0}^{n-1} f_{\text{in}}(i)T + f_{\text{in}}(n)(t-\frac{x-\xi}{v}-nT) & \text{if } nT+\frac{x-\xi}{v} \le t \le (n+1)T+\frac{x-\xi}{v} \\ \sum_{i=0}^{n-1} f_{\text{in}}(i)T + \rho_c v(t-(n+1)T-\frac{x-\xi}{v}) & \text{otherwise } \left(\text{if } t > (n+1)T+\frac{x-\xi}{v}\right) \end{cases} \tag{16}$$

$$\mathbf{M}_{\beta_n} = \begin{cases} +\infty & \text{if } t \le nT + \frac{x-\chi}{w} \\ \sum_{i=0}^{n-1} f_{\text{out}}(i)T + f_{\text{out}}(n)(t-\frac{x-\chi}{w}-nT) & \\ \qquad - \sum_{k=0}^{k_{\max}} \rho(k)X - \rho_m(x-\chi) & \text{if } nT+\frac{x-\chi}{w} \le t \le (n+1)T+\frac{x-\chi}{w} \\ \sum_{i=0}^{n} f_{\text{out}}(i)T - \sum_{k=0}^{k_{\max}} \rho(k)X & \\ \qquad + \rho_c v\left(t-(n+1)T-\frac{x-\chi}{w}\right) & \text{otherwise } \left(\text{if } t > (n+1)T+\frac{x-\chi}{w}\right) \end{cases} \tag{17}$$

Model Constraints

Define the decision variable associated with the value conditions in equations (12), (13), and (14) as

$$y := (\rho(1), \dots, \rho(k_{\max}), f_{\text{in}}(1), \dots, f_{\text{in}}(n_{\max}), f_{\text{out}}(1), \dots, f_{\text{out}}(n_{\max})) \tag{18}$$

Also, denote by $\mathcal{Y}$ the vector space of these decision variables y.

With the explicit solutions in equations (15), (16), and (17), we can determine the physical constraints on this solution space $\mathcal{Y}$ that are implied by the LWR PDE (equation (6)) as the set of linear inequalities below, following the *inf-morphism* property (as in equation (11)):

$$\begin{cases} \mathbf{M}_{M_k}(0, x_p) \geq M_p(0, x_p) & \forall (k,p) \in \mathbb{K}^2 \\ \mathbf{M}_{M_k}(pT, \chi) \geq \beta_p(pT, \chi) & \forall k \in \mathbb{K}, \forall p \in \mathbb{N} \\ \mathbf{M}_{M_k}(\frac{\chi - x_{k+1}}{v}, \chi) \geq \beta_p(\frac{\chi - x_{k+1}}{v}, \chi) & \forall k \in \mathbb{K}, \forall p \in \mathbb{N} \text{ s.t } \frac{\chi - x_{k+1}}{v} \in [pT, (p+1)T] \\ \mathbf{M}_{M_k}(pT, \xi) \geq \gamma_p(pT, \xi) & \forall k \in \mathbb{K}, \forall p \in \mathbb{N} \\ \mathbf{M}_{M_k}(\frac{\xi - x_k}{w}, \xi) \geq \gamma_p(\frac{\xi - x_k}{w}, \xi) & \forall k \in \mathbb{K}, \forall p \in \mathbb{N} \text{ s.t } \frac{\xi - x_k}{w} \in [pT, (p+1)T] \end{cases} \tag{19}$$

$$\begin{cases} \mathbf{M}_{\gamma_n}(pT, \xi) \geq \gamma_p(pT, \xi) & \forall (n,p) \in \mathbb{N}^2 \\ \mathbf{M}_{\gamma_n}(pT, \chi) \geq \beta_p(pT, \chi) & \forall (n,p) \in \mathbb{N}^2 \\ \mathbf{M}_{\gamma_n}(nT + \frac{\chi - \xi}{v}, \chi) \geq \beta_p(nT + \frac{\chi - \xi}{v}, \chi) & \forall (n,p) \in \mathbb{N}^2 \text{ s.t } nT + \frac{\chi - \xi}{v} \in [pT, (p+1)T] \end{cases} \tag{20}$$

$$\begin{cases} \mathbf{M}_{\beta_n}(pT, \xi) \geq \gamma_p(pT, \xi) & \forall (n,p) \in \mathbb{N}^2 \\ \mathbf{M}_{\beta_n}(nT + \frac{\chi - \xi}{w}, \xi) \geq \gamma_p(nT + \frac{\chi - \xi}{w}, \xi) & \forall (n,p) \in \mathbb{N}^2 \text{ s.t } nT + \frac{\chi - \xi}{w} \in [pT, (p+1)T] \\ \mathbf{M}_{\beta_n}(pT, \chi) \geq \beta_p(pT, \chi) & \forall (n,p) \in \mathbb{N}^2 \end{cases} \tag{21}$$

For a full derivation of these inequalities, refer to (*21*).

Notice that because the solutions described in equations (12)-(14) associated with the given value conditions are all linear in y, all of these constraints described by (19)-(21) are also linear in y. We can therefore represent the model constraints in the matrix form

$$A_{\text{model}} y \leq b_{\text{model}} \tag{22}$$

Data Constraints

While the previously described "model constraints" encode the limitations due to the physics of traffic flow, they do not add any new information about the existing state of a system. To estimate boundary conditions such that all known measurements will be satisfied by the derived solution, we must define a separate set of "data constraints". This requires explicit formulation of the sensor data in terms of decision variable y.

To preserve convexity in the resulting optimization problem, data constraints can often be represented as convex inequalities which account for errors inherent in practical measurement techniques. Here we will furthermore assume that all data constraints are linear; they are therefore represented in general as

$$C_{\text{data}} y \leq d_{\text{data}} \tag{23}$$

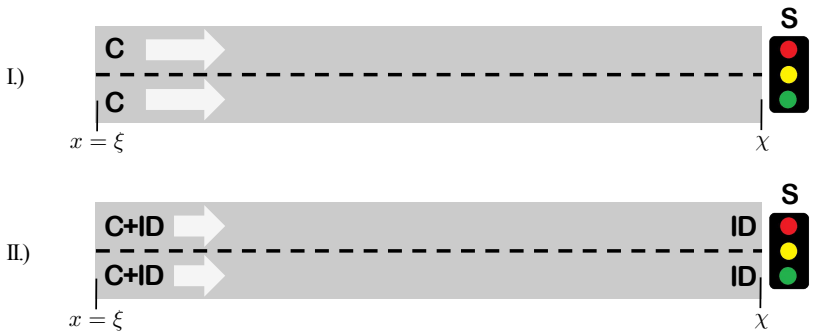

FIGURE 1 Sensor configurations investigated in this work. C denotes an available count measurement; ID denotes a sensor with vehicle identification capabilities for travel time measurements.

Here we investigate the following specific sensor configuration scenarios, which are illustrated in Figure 1:

Scenario I: Detectors providing vehicle counts are placed at the upstream boundary of the link, providing vehicle count measurements that can be aggregated into flow estimates $\bar{f}^k(T, \xi)$ for a fixed time step T. These measured flows have known error percentage $\bar{e_f}$. Because signal timings are known, partial information about link outflow is also available.

Relevant Data Constraints:

- $f_{\text{out}}(t_{\text{red}}) = 0$
- $(1 - \bar{e_f})\bar{f}^k(t_k, \xi) \leq f_{\text{in}}(k) \leq (1 + \bar{e_f})\bar{f}^k(t_k, \xi) \quad \forall\, t_k \in [k \cdot T, (k+1) \cdot T]$

Scenario II: Flow measurements as in Scenario I are given. Additionally, re-identification sensors placed at the upstream and downstream ends of the link provide point-to-point travel times $\bar{t}$ with maximum error $\bar{e_t}$, corresponding to exit time stamps $\bar{t_f}$ for 5-15% of the vehicles traveling across the link.

Relevant Data Constraints:

- $f_{\text{out}}(t_{\text{red}}) = 0$
- $(1 - \bar{e_f})\hat{f}^k(t_k, \xi) \leq f_{\text{in}}(k) \leq (1 + \bar{e_f})\bar{f}^k(t_k, \xi) \quad \forall\, t_k \in [k \cdot T, (k+1) \cdot T]$
- $M(\bar{t_f} - \bar{t} - \bar{e_t}, \xi) \leq M(t_f, \chi) \leq M(\bar{t_f} - \bar{t} + \bar{e_t}, \xi)$ for $\bar{t}$, $\bar{t_f}$ sampled from 5-15% of exiting vehicles

Estimation of Unobservable Boundary Flows

To estimate the unknown or uncertain boundary conditions, we formulate an objective problem over space $\mathcal{Y}$ with the model constraints in equations (19)-(21) and data constraints corresponding

to any available measurements:

$$\text{Minimize (or Maximize):} \quad g(y) \tag{24}$$
$$\text{subject to:} \quad \begin{cases} A_{\text{model}} y \leq b_{\text{model}} \\ C_{\text{data}} y \leq d_{\text{data}} \end{cases}$$

The objective $g(y)$ can be any convex piecewise affine function of the decision variable. However if limited availability of data suggests a highly underdetermined problem, the objective should be crafted to ensure realism in the resulting solution.

For example, the scenarios investigated in this work do not include full constraints on outflows via measurements; they only assume zero outflow when impeded by a signal. Therefore many feasible solutions y with various exiting flow profiles can satisfy the existing constraints. But because drivers usually act to maximize their velocity whenever possible, we should prefer solutions where rapid outflow is encouraged. This is achieved by maximizing the sum of outflows weighted by a small, decreasing function $\mu(n)$:

$$\max_{y \in \mathcal{Y}} \quad \sum_n \mu(n) f_{\text{out}}(n) \tag{25}$$
$$\text{subject to:} \begin{cases} A_{\text{model}} y \leq b_{\text{model}} \\ f_{\text{out}}(t_{\text{red}}) = 0 \\ \text{[other data constraints]} \end{cases}$$

Queue Calculation

Ultimately, the optimal initial/boundary conditions $y^* = \arg\max(g(y))$ are used to determine the solution of the Moskowitz function explicitly via equations (15) - (17). The integer level-sets of the resulting piecewise linear function $\mathbf{M}(t.x)$ represents "modeled" vehicle trajectories. Multiple link performance metrics can be estimated from this result, including queue lengths. Two criteria will identify queues:

- Point density is maximized: $\rho(t,x) = \left| \frac{\partial \mathbf{M}(t,x)}{\partial x} \right| = \rho_j \pm \delta$
- Point flow is zero: $f(t,x) = \frac{\partial \mathbf{M}(t,x)}{\partial t} \approx 0$

The first criterion (maximum density) is a more reliable indicator of queued state than zero flow, as the latter may also occur when the link is entirely empty. We therefore define the instantaneous queue length as the location of the boundary between areas of jam density and areas of lesser density at each time t.

DATA

We ran our estimation algorithm on data from NGSIM's Lankershim dataset, available online at http://ngsim-community.org/. The sample was collected on Lankershim Boulevard in Los Angeles, California; the deployment site is illustrated in Figure 2.

Detailed trajectory data originates from video obtained from five high-definition cameras monitoring a 1,600-foot stretch of road from 0828 to 0900 on June 16, 2005. During this period, 2,442 vehicles were detected within the monitored area; their trajectories were transcribed at a time resolution of 10 samples/second. According to NGSIM documentation, trajectory points

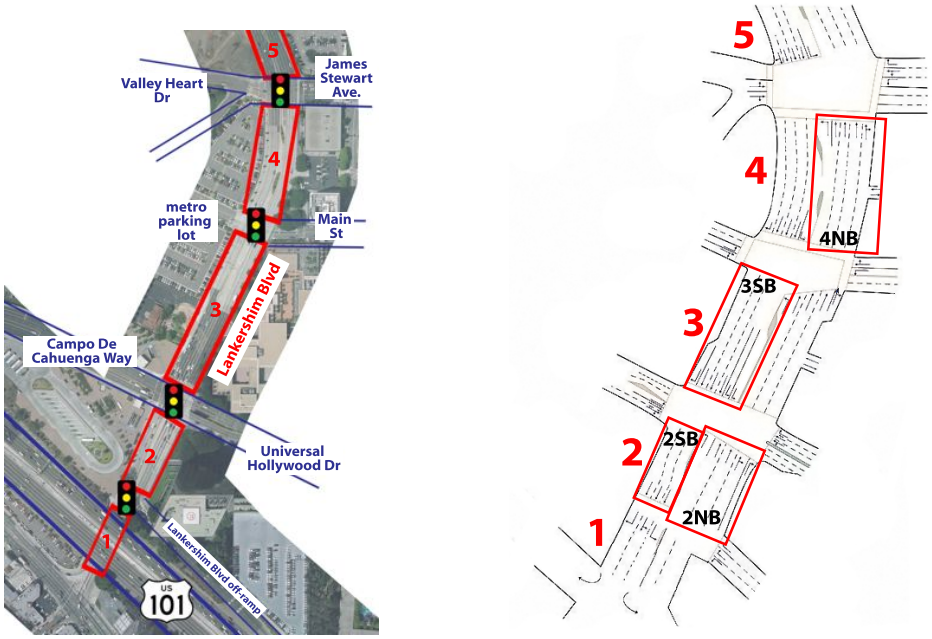

FIGURE 2 High-resolution vehicle trajectories are available for 5 blocks of Lankershim Blvd. We tested our algorithm on the highlighted links, which are representative of multiple typical link geometries: 2 northbound, 2 southbound, 3 southbound, and 4 northbound.

are considered accurate up to a 4 ft. radius; we have no reason to believe that this amount of error would affect our quantitative queue length comparisons–especially as it is assumed consistent among concurrent vehicles.

We simulated count sensors at the immediate upstream end of each link by extracting all timestamps at which a vehicle enters the link from the adjacent intersection. Flow measurements were then estimated by aggregating these "counts" within every five-second time period. We extracted travel time measurements from randomly sampled trajectories, where entry and exit times correspond to the timestamps at which the sampled vehicles were first and last detected on the relevant link. Note that the time a vehicle spent within the surrounding intersections is not included in the travel time samples. Red signal times were extracted from the signal timing plans provided in the NGSIM database.

For demonstration of our algorithm, we chose to analyze data from the four links highlighted in Figure 2:

- link 2 southbound, a 3-lane link between a busy cross-street and a signalized intersection with no possible turn movements;
- link 2 northbound, a 3-lane link that expands to 5 lanes downstream with one designated left-turn lane and two permissive right-turn lanes;
- link 3 southbound, a link with three through-lanes, two left-turn lanes, and a right-turn pocket;
- link 4 northbound, a 4-lane link with an intermediate entry-exit point and a small left-turn pocket at the downstream end.

These links were chosen to be representative of a variety of physical features, such as both specialized and shared turn lanes, and intermediate entry/exit points.

Calibration of the fundamental diagram parameters v, w, and f_c was performed via visual inspection of the trajectories. The following values were used for all links:

- free-flow velocity, v = 15.64 meters/sec (35 miles/hour)
- shockwave velocity, w = -6.70 meters/sec (-15 miles/hour)
- critical density, ρ_c = 0.375 vehs/meter (60 vehs/mile)
- jam density, $\rho_j = \rho_c(1 + \frac{v}{w})$ = 0.125 vehs/meter (200 vehs/mile)

These parameters correspond to the dynamics of a single lane. To ensure that the "measured" input flows are treated consistently, the calculated flows were scaled by the inverse of the number of lanes at link entry. Results are therefore intended to represent an "average" queuing behavior on each of the links, and not expected to exactly match the behavior observed on any one lane. We also chose common values for measurement error:

- Count sensors are accurate within 5%.
- Travel time estimates have a maximum error of 0.5 seconds.

In the following section, estimated queue lengths are compared to directly-measured queues from ten signal cycles for each of four link-directions.

NUMERICAL RESULTS

We solved the relevant linear programs using a MATLAB-based optimization software package. We then used a separate MATLAB toolbox to generate the desired B-J/F solutions to the Moskowitz HJ-PDE (*34*). This LWR toolbox is available at http://traffic.berkeley.edu/project/downloads/lwrsolver.

We ran this code on each of the four link-directions shown in Figure 2 for all sensor configuration scenarios. Specifically, we compared the time-resolved queue length estimates generated from the calculated Moskowitz solutions to those detected in the data. In the data, we define the back of a queue as the location of the car with the highest entry index that is stopped on a link at a given time. Because vehicles tended to "drift" slightly when in a queue, this detection method was not always accurate; discontinuities in detected queue lengths sometimes caused unrealistic noise in the resulting queue length error calculations.

Scenario I: Upstream Flows and Signals

Figure 3 illustrates a sample of the results of our estimation algorithm on Link 2 SB, a 3-lane link with simple geometry with no possible downstream turn movements.

With this basic lane geometry and low demands, we see that the modeled trajectory behavior closely follows an "average" of the three exiting lanes. However it fails to replicate the excessive queueing (and possible spillover) seen on lane 3 at 1300 seconds. Replication of such extreme queuing occurring only in a single lane is not expected given the lane-averaged flows input into the model. To achieve a more accurate representation of true behavior, one may need to access lane-specific flow sensors and run this model on each lane independently. This procedure, however, would likely be sensitive to lane-changing behaviors and inaccuracies in turn ratio estimation.

Achieving similarly accurate queue length results on links with complicated geometries

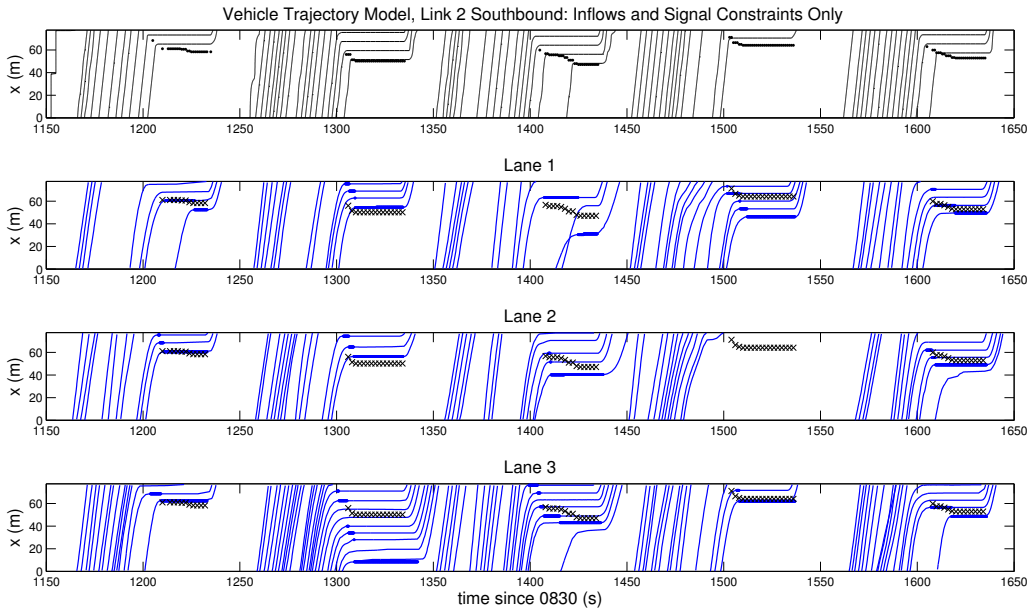

FIGURE 3 Modeled and ground-truth trajectories for a sample time period. Inflows and constrained (zero) outflows were imposed. For visual comparison, the queue lengths estimated by the PDE model are shown on all data plots.

and downstream turn movements requires additional processing. Link 2 NB, for example, is a link with two through-only lanes, one shared through-right turn lane, one right turn only lane, and one left turn only lane, as seen in Figure 2. We used aggregate inflows from the three lanes present at the upstream end of the link, and restricted modeled outflows according to signal timings which restricted through movement at the downstream end. We also assumed that flows were evenly divided between the three through movement lanes, and therefore divided inflows by three before modeling.

However the resulting trajectories, such as those shown in Figure 4, tended to overestimate the queues in all of the through lanes. These results suggested that it was necessary to further reduce the inflow measurements used in the modeling process to account for the turning flows, which not only entered downstream queues disproportionately but also were restricted by different signal timings than those of the through-flows. We therefore reduced the measured inflows by the estimated percentage of turning vehicles before processing data constraints .

For example, in the case of link 2 NB we determined that over the entire 30-minute study period, approximately 4% of vehicles exiting the link in this direction turned left and 20% turned right. Hence we reduced inflows by 24%, and re-ran the optimization and PDE solution procedures. The trajectories modeled using the lesser inflows were more representative of the average behavior seen on all through-only lanes, as can be seen in Figure 4. Note that while we were able to "predict" turn ratios fairly accurately in this work via analysis of our detailed data set, similar procedure can be followed in practice using turning ratio estimates determined by previous local surveying or OD-estimation techniques.

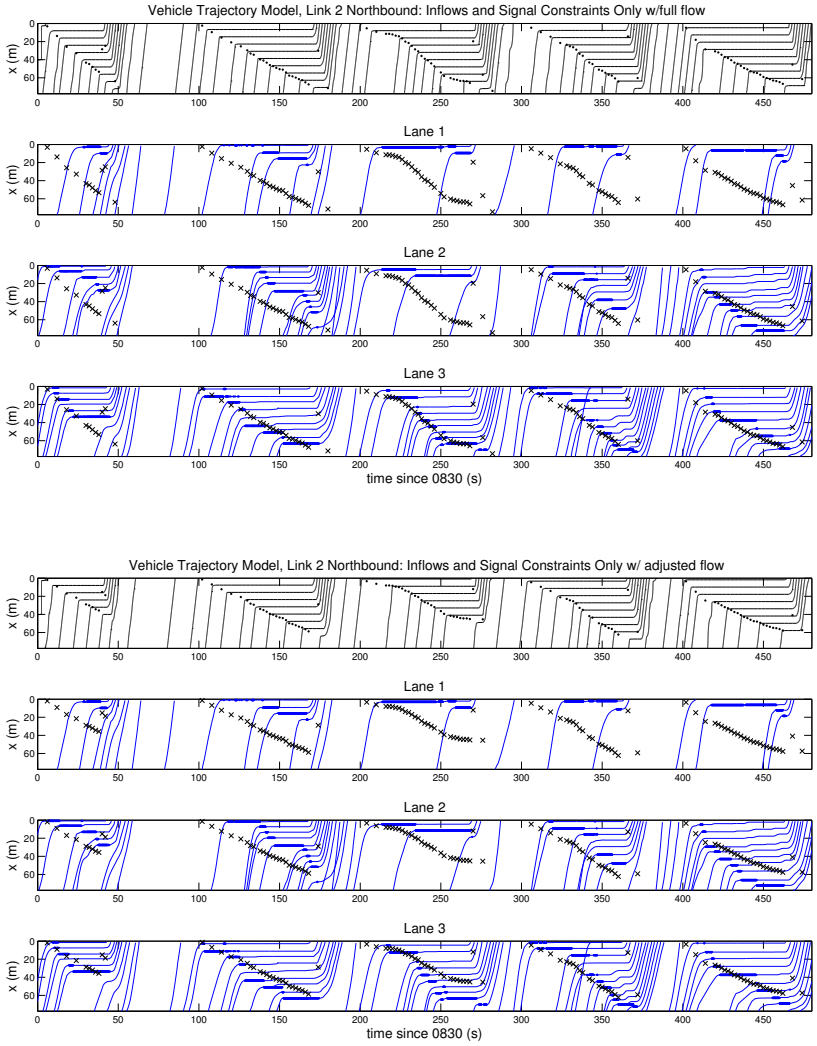

FIGURE 4 Top: Algorithm demonstrated on Link 2NB with turning lanes present and no inflow adjustments. Bottom: Model performance on Link 2NB with inflow reduced by 24%, to be representative of through movements only.

Figure 5 demonstrates similarly successful results on the through-only lanes of Link 3 southbound, a block with two dedicated left-turn lanes and a third dedicated right-turn lane.

The estimation error function, illustrated in Figure 6, reveals that while the accuracy of the queue length estimate varies significantly between lanes, link-average error remains very low–within ± 16 meters, or two car lengths at maximum density $\rho_j = 0.125$ vehicles/meter. These results were typical of instances where there was no abnormal disturbances such as a long truck or turn lane spillover on any lanes of the link. There is no evidence that queues are systematically over-estimated or underestimated, or that the estimated lengths are consistently less accurate at either the beginning or end of a queueing cycle using this technique.

In our study of Link 4 NB, we expected that the intermediate entry/exit point would cause error in both modeled queue lengths because this comprised an obvious violation in the mass

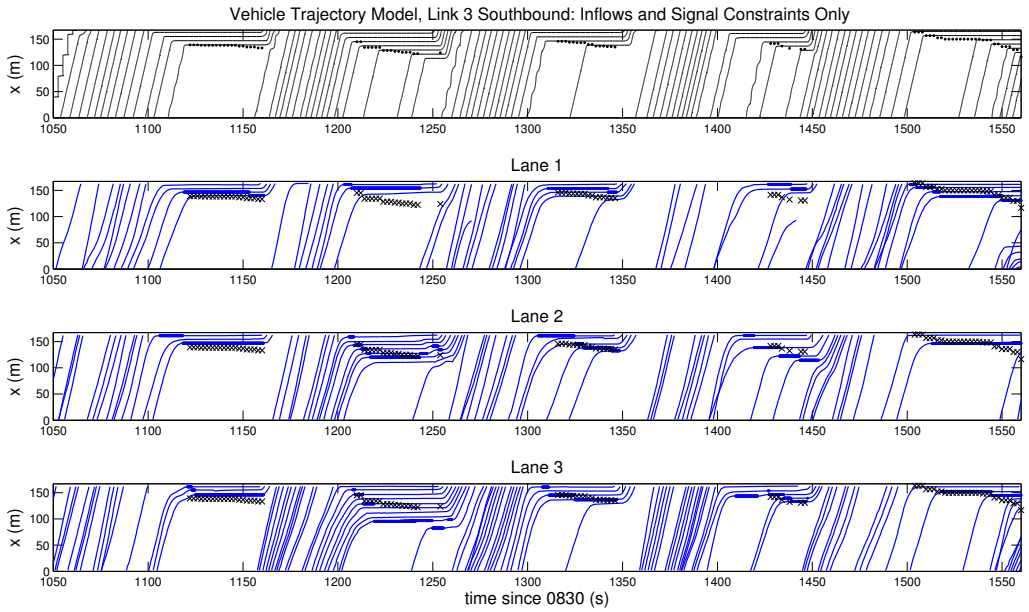

FIGURE 5 Model performance on through lanes of Link 3 SB. Inflow was reduced by 36% to account for turning vehicles. Modeled queues are represented in bold lines on all plots.

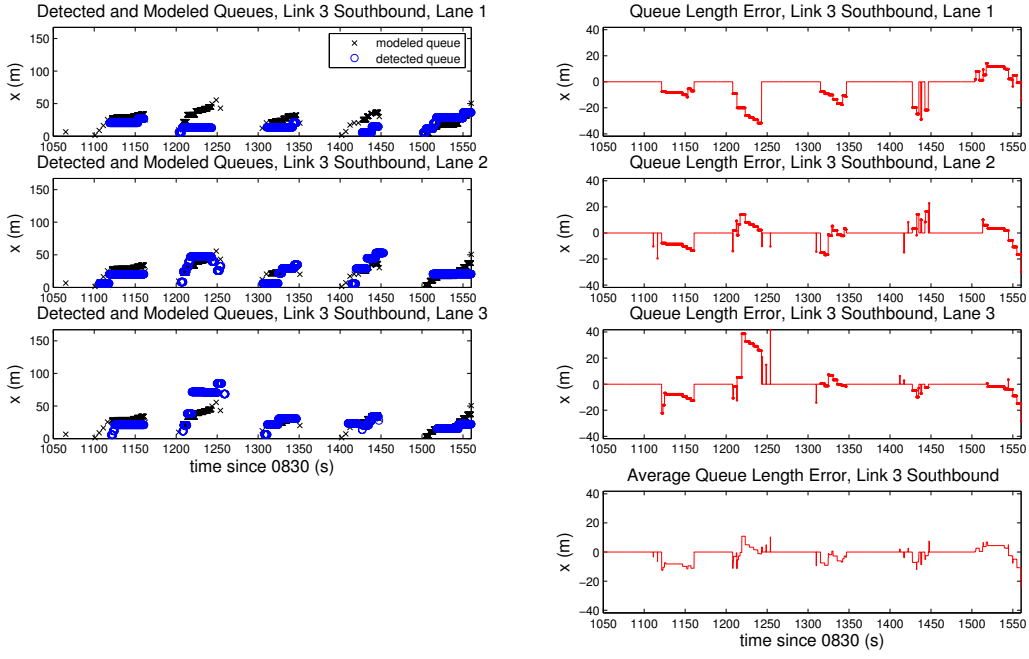

FIGURE 6 A comparison of modeled queues to detected queues. Average queue length error remains under 16 meters, or < 2 vehicles at jam density $\rho_j = 0.125$ vehicles/meter.

conservation assumption of the underlying LWR model. However, the level of flows exiting and entering the link did not constitute a significant percentage of link flows in the samples we studied, and thus the results were not notably affected by such violation.

Scenario II: Upstream Flows, Signals, and Travel Times

The additional constraints due to travel time measurements as described in Scenario II initially caused the boundary condition optimization function to become over-constrained and thus infeasible. This is due to the flow and queue aggregation assumed in our implementation. For example, Figure 3 illustrates a situation where a vehicle entering Lane 3 of Link 2 at 1300 seconds would encounter a dramatically different queue (and thus experience a significantly different travel time) than a vehicle concurrently entering Lane 2 of the same link. If conflicting travel times were sampled, the corresponding conflicting constraints would cause the problem to become unsolvable.

Without studying individual lane behaviors, we were therefore constrained to using very small penetration rates which did not contain samples which conflicted outside the range of permissible error. We also made a further adjustment in the solution procedure: in addition to the 0.5 second error permitted in travel time measurements, we added a 0.25-vehicle error on the solution of the Moskowitz function directly. This effectively modified a travel time constraint to the following:

$$M(\bar{t_f} - \bar{t} - \bar{e_t}, \xi) - 0.25 \leq M(\bar{t_f}, \chi) \leq M(\bar{t_f} - \bar{t} + \bar{e_t}, \xi) + 0.25 \tag{26}$$

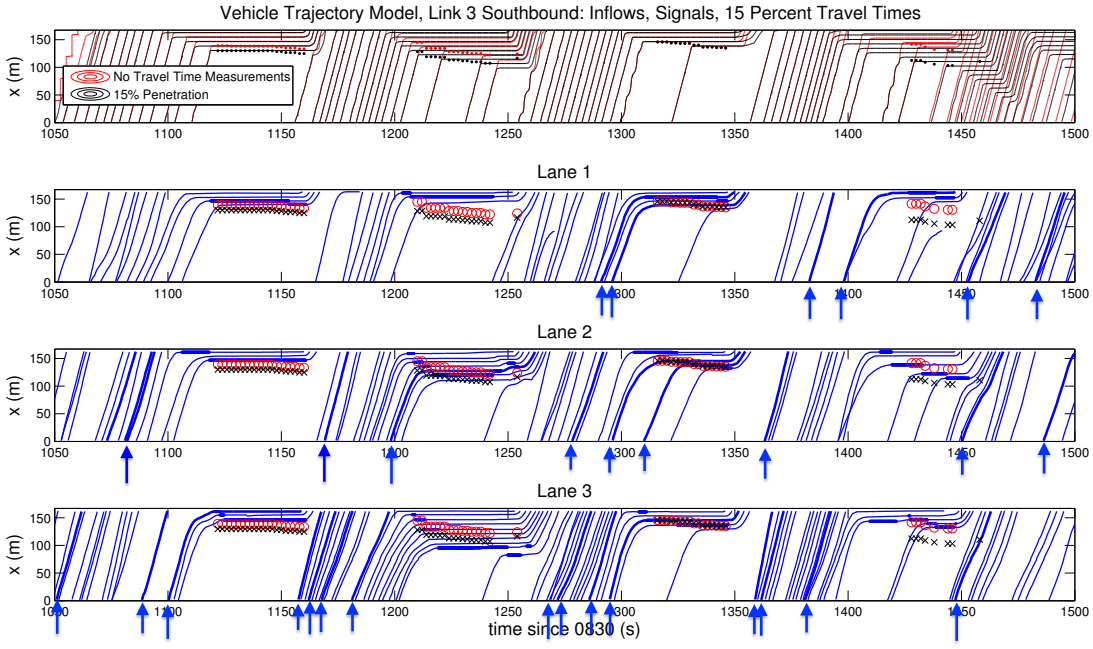

FIGURE 7 The trajectories from which travel times were sampled are highlighted with an arrow at time of entry. Several "outlier" trajectories from the end of the queues on Lanes 2 and 3 caused an adjustment in the modeled queue for the first, second, and fourth light cycles.

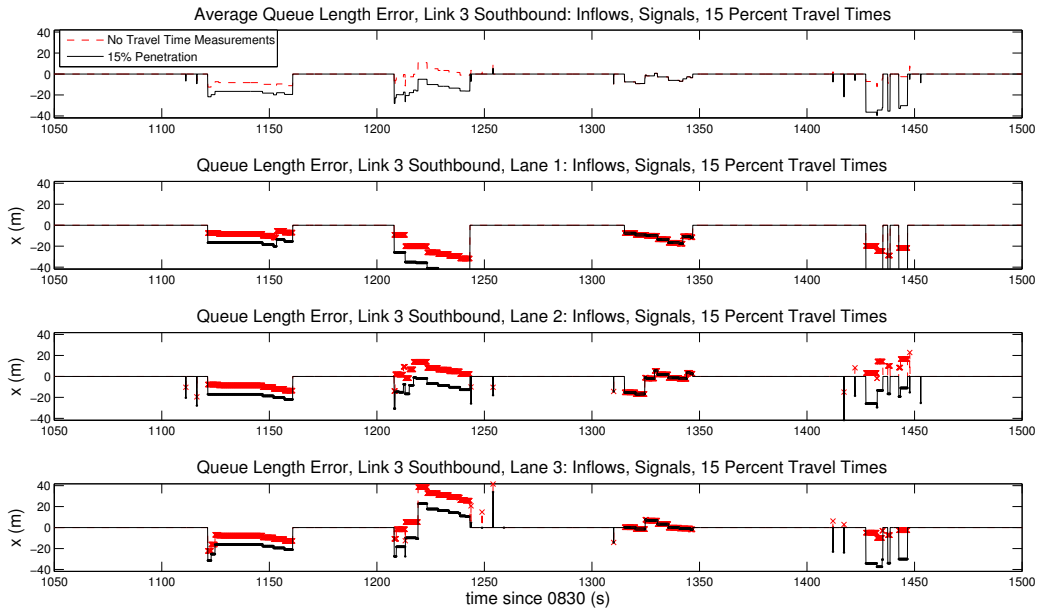

FIGURE 8 Travel time samples decreased the error for some lanes as they "tuned" the output to those lanes for specific queue cycles. However, the estimates were often made worse for the other lanes, causing increased error in the average length estimates for the affected cycles.

While these adjustments to the boundary condition algorithm allowed for the identification of feasible solutions, they also minimized the impact of travel time measurements on the resulting trajectories and queue lengths. We found that with realistic penetration rates of 5-15%, the addition of travel time estimates did little to improve the accuracy of modeled queue lengths. In most common congestion patterns with well-distributed flow, the additional constraints were already satisfied by the solution found in Scenario I and thus did not have any impact on the resulting trajectories. When additional active constraints were imposed by travel time samples, they did not typically improve the lane-averaged error in queue length estimates. See for example the trajectories on Link 3SB shown in Figures 7 - 8.

From the comparison of the error resulting from estimates of the two sensor scenarios in Table 1 below, it is clear that travel time measurements do not consistently provide useful information beyond that available with just inflow and signal timing information.

TABLE 1 Average Absolute Error in Queue Length Estimates

Link	Scenario 1	Scenario 2 (15%)
2 SB	9.88 m	9.88 m
2 NB	14.73 m	19.30 m* (w/ 5%)
3 SB	13.69 m	15.53 m
4 NB	11.67 m	11.67 m

The best results for both scenario were observed in Link 2SB, the link with no turn movements to cause differentiation in lane behaviors. In contrast, Link 2NB is a short link with both

left and right turn movements; it is likely that the rapid lane changing and queue blocking of the turning vehicles cause the exaggerated error seen in our model results. Note that because of this significant variance between queues on the three through lanes of this link, we were unable to find ten queue cycles where it was feasible to satisfy the constraints of a 15% travel time sample. Hence the value listed in Table 1 represents results for a 5% travel time penetration rate.

FUTURE WORK

Future work should use this method to examine the use of travel time measurements in combination with different fixed sensor configurations and link geometries to examine where and when such measurements would beneficially contribute to the resulting queue estimates. We hypothesize that longer arterial links may exhibit more uniform queue lengths on all lanes with similar turn movements; travel time samples could therefore be more beneficial as the link length gets larger. The authors also plan to extend this LWR-based estimation method beyond a single link to a series of networked arterial links. This would eventually contribute to a tool that can be used to develop and implement model-predictive control algorithms with real-time sensor feedback on an arterial traffic network.

ACKNOWLEDGEMENT

This work was funded by the California Department of Transportation under the Connected Corridors program. We would like to acknowledge Pravin Variaya for his advice and suggestions regarding the applications of this work. The Lankershim Blvd. dataset is attributed to NGSIM and FHWA.

REFERENCES

[1] Papageorgiou, M., C. Kiakaki, V. Dinopoulou, A. Kotsialos, and Y. Wang. Review of road traffic control strategies. *Proceedings of the IEEE*, Vol. 91, No. 12, 2003, pp. 2043–2067.

[2] Hunt, P., D. Robertson, R. Bretherton, and R. Winton, *SCOOT-a traffic responsive method of coordinating signals*, 1981.

[3] Varaiya, P., The Max-Pressure Controller for Arbitrary Networks of Signalized Intersections. In *Advances in Dynamic Network Modeling in Complex Transportation Systems* (S. V. Ukkusuri and K. Ozbay, eds.), Springer New York, New York, NY, 2013, pp. 27–66.

[4] Sun, X. and R. Horowitz. Set of New Traffic-Responsive Ramp-Metering Algorithms and Microscopic Simulation Results. *Transportation Research Record: Journal of the Transportation Research Board*, Vol. 1959, 2006, pp. 9–18.

[5] Sanchez, R. O., R. Horowitz, and P. Varaiya. Analysis of Queue Estimation Methods Using Wireless Magnetic Sensors. *Transportation Research Record: Journal of the Transportation Research Board*, Vol. 2229, 2011, pp. 34–45.

[6] Liu, H. X., X. Wu, and P. G. Michalopoulos. Improving Queue Size Estimation for Minnesota's Stratified Zone Metering Strategy. *Transportation Research Record: Journal of the Transportation Research Board*, Vol. 2012, 2007, pp. 38–46.

[7] Wu, J., X. Jin, A. J. Horowitz, and D. Gong. Experiment to Improve Estimation of Vehicle Queue Length at Metered On-Ramps. *Transportation Research Record: Journal of the Transportation Research Board*, Vol. 2099, 2009, pp. 30–38.

[8] Vigos, G., M. Papageorgiou, and Y. Wang. Real-time estimation of vehicle-count within signalized links. *Transportation Research Part C: Emerging Technologies*, Vol. 16, No. 1, 2008, pp. 18–35.

[9] Wu, J., X. Jin, and A. J. Horowitz. Methodologies for Estimating Vehicle Queue Length at Metered On-Ramps. *Transportation Research Record: Journal of the Transportation Research Board*, Vol. 2047, 2008, pp. 75–82.

[10] Viti, F. and H. Van Zuylen. The Dynamics and the Uncertainty of Queues at Fixed and Actuated Controls: A Probabilistic Approach. *Journal of Intelligent Transportation Systems*, Vol. 13, No. 1, 2009, pp. 39–51.

[11] Kwong, K., R. Kavaler, R. Rajagopal, and P. Varaiya. Arterial travel time estimation based on vehicle re-identification using wireless magnetic sensors. *Transportation Research Part C: Emerging Technologies*, Vol. 17, No. 6, 2009, pp. 586 – 606.

[12] Sanchez, R., C. Flores, R. Horowitz, R. Rajagopal, and P. Varaiya, Vehicle re-identification using wireless magnetic sensors: Algorithm revision, modifications and performance analysis. In *Vehicular Electronics and Safety (ICVES), 2011 IEEE International Conference on*, 2011, pp. 226 –231.

[13] Sanchez, R. O., *Wireless Magnetic Sensor Applications in Transportation Infrastructure*. Ph.D. thesis, University of California, Berkeley, 2012.

[14] Olszewski, P. S. Modeling probability distribution of delay at signalized intersections. *Journal of Advanced Transportation*, Vol. 28, No. 3, 1994, pp. 253–274.

[15] Geroliminis, N. and A. Skabardonis. Prediction of arrival profiles and queue lengths along signalized arterials by using a Markov decision process. *Transportation Research Record: Journal of the Transportation Research Board*, Vol. 1934, 2005, pp. 116–124.

[16] Furtlehner, C. and J.-M. L. A. de La Fortelle, A Belief Propagation Approach to Traffic Prediction using Probe Vehicles. In *The 10th International IEEE Conference on Intelligent Transportation Systems*. Seattle, WA, USA, 2007.

[17] Hellinga, B., P. Izadpanah, H. Takada, and L. Fu. Decomposing travel times measured by probe-based traffic monitoring systems to individual road segments. *Transportation Research Part C: Emerging Technologies*, Vol. 16, No. 6, 2008, pp. 768–782.

[18] Comert, G. and M. Cetin. Queue length estimation from probe vehicle location and the impacts of sample size. *European Journal of Operational Research*, Vol. 197, No. 1, 2009, pp. 196 – 202.

[19] Thiagarajan, A., L. Ravindranath, K. LaCurts, S. Madden, H. Balakrishnan, S. Toledo, and J. Eriksson, VTrack: accurate, energy-aware road traffic delay estimation using mobile phones. In *7th ACM Conference on Embedded Networked Sensor Systems*. ACM, Berkeley, CA, USA, 2009, pp. 85–98.

[20] Stephanopoulos, G., P. G. Michalopoulos, and G. Stephanopoulos. Modelling and analysis of traffic queue dynamics at signalized intersections. *Transportation Research Part A: General*, Vol. 13, No. 5, 1979, pp. 295–307.

[21] Canepa, E. S. and C. Claudel. Exact solutions to traffic density estimation problems involving the Lighthill-Whitham-Richards traffic flow model using Mixed Integer Programming, 2012, pp. 832–839.

[22] Lighthill, M. J. and G. B. Whitham. On kinematic waves. II. A theory of traffic flow on long crowded roads. *Proceedings of the Royal Society of London. Series A. Mathematical and Physical Sciences*, Vol. 229, No. 1178, 1955, pp. 317–345.

[23] Richards, P. I. Shock waves on the highway. *Operations Research*, Vol. 4, No. 1, 1956, pp. 42–51.

[24] Skabardonis, A. and N. Geroliminis. Real-Time Monitoring and Control on Signalized Arterials. *Journal of Intelligent Transportation Systems*, Vol. 12, No. 2, 2008, pp. 64–74.

[25] Geroliminis, N., Queue spillovers in city street networks with signal-controlled Intersections. In *89th Transportation Research Board Annual Meeting*. Washington, DC, USA, 2010.

[26] Moskowitz, K. and L. Newan. Notes on freeway capacity. *Highway Research Record*, 1963, pp. 44–68.

[27] Frankowska, H. Lower semicontinuous solutions of Hamilton-Jacobi-Bellman equations. *SIAM Journal on Control and Optimization*, Vol. 31, No. 1, 1993, pp. 257–272.

[28] Tampere, C., S. P. Hoogendoorn, and B. van Arem. A Behavioural Approach to Instability, Stop and Go Waves, Wide Jams and Capacity Drop. *Transportation and traffic theory*, Vol. 16, 2005, pp. 205–228.

[29] Work, D. B., S. Blandin, O. P. Tossavainen, B. Piccoli, and A. M. Bayen. A Traffic Model for Velocity Data Assimilation. *Applied Mathematics Research eXpress*, 2010.

[30] Blandin, S., A. Couque, A. Bayen, and D. Work. On sequential data assimilation for scalar macroscopic traffic flow models. *Physica D*, Vol. 241, No. 17, 2012, pp. 1421–1440.

[31] Claudel, C. and A. M. Bayen. Lax–Hopf Based Incorporation of Internal Boundary Conditions into Hamilton-Jacobi Equation. Part I: Theory. *Automatic Control, IEEE Transactions on*, Vol. 55, No. 5, 2010, pp. 1142–1157.

[32] Aubin, J.-P., A. M. Bayen, and P. Saint-Pierre. Dirichlet Problems for some Hamilton–Jacobi Equations with Inequality Constraints. *SIAM Journal on Control and Optimization*, Vol. 47, No. 5, 2008, pp. 2348–2380.

[33] Claudel, C. and A. M. Bayen. Convex Formulations of Data Assimilation Problems for a Class of Hamilton–Jacobi Equations. *SIAM Journal on Control and Optimization*, Vol. 49, No. 2, 2011, pp. 383–402.

[34] Mazaré, P.-E., A. H. Dehwah, C. Claudel, and A. M. Bayen. Analytical and grid-free solutions to the Lighthill-Whitham-Richards traffic flow model. *Transportation Research Part B*, Vol. 45, No. 10, 2011, pp. 1727–1748.